Mechanical Systems and Signal Processing 151 (2021) 107350

Contents lists available at ScienceDirect

Mechanical Systems and Signal Processing

journal homepage: www.elsevier.com/locate/ymssp

Vibration control with piezoelectric elements: The indirect measurement of the modal capacitance and coupling factor

M. Berardengo [a,b,*], S. Manzoni [c], J. Høgsberg [d], M. Vanali [b]

[a] Universitá degli Studi di Genova, Department of Mechanical, Energy, Management and Transportation Engineering, Via Opera Pia, 15A – 16145 Genoa, Italy
[b] Universitá degli Studi di Parma, Department of Engineering and Architecture, Parco Area delle Scienze, 181/A – 43124 Parma, Italy
[c] Politecnico di Milano, Department of Mechanical Engineering, Via La Masa, 34 - 20156 Milan, Italy
[d] Technical University of Denmark, Department of Mechanical Engineering, Nils Koppels Allé, building 403, DK-2800 Kongens Lyngby, Denmark

ARTICLE INFO

Article history:
Received 15 May 2020
Received in revised form 3 August 2020
Accepted 3 October 2020

Keywords:
Vibration control
Modal capacitance
Coupling factor
Piezoelectric shunt
Negative capacitance
Resonant shunt

ABSTRACT

The knowledge of the modal capacitance and electro-mechanical coupling factor is essential for a proper design of systems with embedded piezoelectric transducers and materials. In light of this, this paper presents two indirect methods for measuring the piezoelectric modal capacitance and a method to estimate the modal electro-mechanical coupling factor. All methods rely on simple vibration measurements of the structure with the piezoelectric transducer connected to a proper shunt impedance, thus avoiding measurements of piezoelectric current and voltage by expensive equipment. For the modal electro-mechanical coupling factor, the proposed method guarantees reduced uncertainty compared to traditional experimental estimation procedures. Upon introduction of the underlying theory, the paper experimentally demonstrates the reliability and effectiveness of the methods by comparison with well-established procedures.

1. Introduction

Vibration control of structures is a fundamental issue for their durability and performances. This aspect has become even more important in the last decades since many applications rely on lightweight structures subject to a harsh dynamic environment. In these cases, the high vibration level could cause material fatigue, shortening the operating life of the system due to possible damages, and also increase of maintenance costs. Consequently, the reduction of the undesirable vibrations becomes a fundamental issue. In this scenario, piezoelectric materials play an important role because their use does not cause much additional weight, which is a key point for the majority of light structures, they allow to achieve wide control bandwidths and significant forces, they are characterised by low power consumption and can be used both as sensors and actuators and therefore they show attractive features for both active and passive control strategies. Piezoelectric materials have been successfully used for active control in several applications [1], such as in truss structures [2], helicopters [3], spacecrafts [4], satellites [5] and also in civil engineering [6]. A detailed review of recent developments in the field of active vibration control through piezoelectric actuators has been published by Shivashankar and Gopalakrishnan [7].

Particular attention has been paid to the optimisation of the control strategy, by e.g. fuzzy-logic algorithms [8], optimal control [9], multi-objective optimization algorithms [10] or other types of controller [11,12], the geometrical and material parameters [13–15] and the location on the structure to maximise the control effect, while keeping the control effort as

* Corresponding author at: Department of Mechanical, Energy, Management and Transportation Engineering, Via Opera Pia, 15A – 16145 Genoa, Italy.
E-mail address: marta.berardengo@unige.it (M. Berardengo).

https://doi.org/10.1016/j.ymssp.2020.107350
0888-3270/

low as possible [16]. Different algorithms have been employed for the optimisation of the actuator/sensor position on complex structures, such as genetic algorithms [17], model-based linear quadratic regulators [18] or other criteria [19,20]. Optimal configurations have been proposed for different applications, such as the rear wing of a racing car [21] or adaptive trusses [22], and various frequency ranges [23]. The reason why great attention has been paid to these aspects is that the actuation capability depends on the coupling between the strain field and the electrical field [24,25], represented by the electro-mechanical coupling factor [26] that is a function of the electrical, mechanical and geometrical characteristics of the piezoelectric transducer on the structure [27]. This parameter constitutes the foundation of piezoelectric structural control and its estimation is thus important for a proper control design. This is verified by studies that specifically develop methods for the estimation of the coupling coefficient, such as in Chesne et al. [28] where an approach especially effective for small parameter values is presented. The knowledge of the electro-mechanical coupling factor is as well important in other piezoelectric-based applications, for example in energy harvesting, where an accurate estimation of the coupling factor allows for a proper prediction of the effectiveness of the electro-mechanical conversion [29], as further evidenced in e.g. [30,31].

The key role of the coupling factor becomes even more important when passive or semi-passive control is considered, for example in piezoelectric shunt damping [32] or synchronized switch damping [33]. In these cases, the mechanical energy, converted into electrical energy, is reused to properly control the structure. Thus, the performances of these strategies strongly depend on the coupling factor, making its estimation essential for effective tuning of the control parameters to maximize the achievable attenuation. Several studies on this topic have been carried out in the field of piezoelectric shunt damping, where the control action is obtained through the connection of a proper electric impedance (shunt) across the piezoelectric transducer electrodes [34,35], thereby effectively attenuating vibrations in e.g. beams [36] or plates [37]. The control action can be designed for different targets, depending on the type of impedance. The simplest shunt impedances can be composed of a pure resistance [26] or its series/parallel connection with an inductance [38,39]. The tuning of the shunt impedance can rely on different principles, such as pole placement techniques [40,41] or minimisation of the system Frequency Response Function (FRF) [42,43]. Furthermore, multi-branch impedances can be used for multi-mode vibration control, by the current blocking method of Wu [44] or the subsequent current flowing technique proposed by Behrens et al. [45]. Modified versions of these solutions have since been analysed and proposed to improve the previous techniques [46,47]. More complex networks can be used for broadband [48,49], non-linear [50,51] or noise control [52], for control with multiple transducers [53,54], and in different applications for cable damping [55] and vibration isolation [56]. Moreover, synchronized switch damping aims at enhancing the control performance by adding switches to the shunt circuit, based on active elements [57], inductors [58], voltage sources [33], or even periodic impedances [59]. However, in all the above cases, regardless the impedance used and the tuning strategy applied, the accurate estimation of the piezoelectric transducer capacitance and coupling factor is required to effectively tune the control system. Up to few years ago, most of the literature relied on models where the value used for the piezoelectric capacitance was the blocked capacitance, associated with the transducer linked to a blocked structure. However, since a thin structure is usually flexible and exhibits significant dynamic behaviour, this piezoelectric capacitance value coincides with the value at infinite frequency, where the dynamic response of the flexible structure vanishes [60,61]. Therefore, this value of the capacitance will be referred to as C_∞.

Few years ago, it was observed that the use of C_∞ in reduced order models of the electro-mechanical system is not able to provide accurate tuning of the shunt impedance, resulting in non-optimised attenuation performances. Indeed, to achieve an optimal tuning, a modified value of the piezoelectric capacitance must be used, which accounts for the contribution from the neglected modes to the electrical behaviour of the system. Supposing that the control action is focused on the s-th mode of the system, the capacitance value to be used is the modal capacitance C_s that is obtained by adding a correction term C'_s to C_∞. The term C'_s allows to take into consideration the influence of the modes higher than the s-th [60,62]. Moreover, the knowledge of the modal capacitance C_s has been proved to be important for a proper tuning also in case of multi-mode control [63], and not only for single mode control. Despite the importance of the modal capacitance was observed in the field of piezoelectric shunt damping, it plays the same significant role when dealing with active control or energy harvesting since it allows for a more accurate description of the electro-mechanical structure.

Since then, different methods have been proposed in the literature to estimate the modal capacitance. Berardengo et al. [64] proposed to measure the trend of the capacitance of the piezoelectric patch as a function of the frequency and then to fit the experimental data with a model. Toftekær and Høgsberg [65] developed a method based on the measurement of modal charge and voltage. The two methods are based on the same model of the system and thus lead to similar results. Even if the two methods are effective in estimating C_s, both require to measure the current flowing through the piezoelectric transducer. Since this current is very low, dedicated hardware is needed to carry out a reliable measurement, often with the need of expensive impedance analyzers.

To overcome this issue, this paper proposes two alternative methods that allow for an indirect measurement of the modal capacitance C_s. Both are based on the use of simple and inexpensive hardware that is usually present in labs where vibration measurements are performed (e.g. low-cost accelerometers), common acquisition boards and additional inexpensive electronic devices.

Furthermore, taking advantage of the theory behind one of the two methods proposed for the estimation of the modal capacitance, a new method to derive the modal electro-mechanical coupling factor is presented in this paper. As mentioned, the importance of this parameter in piezoelectric control is well known because it is an index of the energy transfer between

the electrical and mechanical parts of the system (e.g. [24]) and several studies focused on its estimation via analytical (e.g. [27]), numerical (e.g. [66]) and experimental (e.g. [24,25]) methods. In general, and especially for complex structures, the most reliable and easy-to-apply experimental procedure is based on the estimation of the short- and open-circuit eigenfrequencies (i.e. with the terminals of the piezoelectric transducer short- and open-circuited, respectively). However, if these two frequencies are really close to each other (i.e. either due to small values of the modal electro-mechanical coupling factor or because the considered mode is at low frequency), the estimation of this coupling coefficient can be significantly affected by the uncertainty on the estimates of the two mentioned eigenfrequencies. The method proposed in this paper is shown to provide an estimate of the coupling coefficient with a reduced uncertainty level compared to the traditional experimental method and, therefore, to provide more accurate results in the most critical situations.

In order to explain the above-mentioned methods, the paper introduces at first the model used for describing the electro-mechanical system in Section 2. This also allows to present one of the methods currently used for estimating C_s, which will be employed in this paper as reference method in order to show the reliability and the effectiveness of the newly proposed techniques. Then, these proposed methods are described in Section 3, while Section 4 explains the new approach for estimating the modal electro-mechanical coupling factor. Finally, Section 5 discusses the experimental campaign carried out to validate the proposed techniques and show their results.

2. System model

The dynamics of a vibrating system with a bonded piezoelectric transducer and excited by an external force f_e (see Fig. 1) can be described, in modal coordinates, by the following equation [26,41]:

$$(-\omega^2 + 2\mathrm{i}\zeta_s\omega_s\omega + \omega_s^2)u_s - \theta_s V = f_{e,s} \quad \text{for} \quad s = 1,\dots,N \tag{1}$$

where ω is the angular frequency, ω_s is the s-th eigenfrequency (with the piezoelectric transducer short-circuited), ζ_s is the associated non-dimensional damping ratio, $f_{e,s}$ is the modal forcing, θ_s is a coupling coefficient per unit modal mass and V is the voltage across the electrodes of the piezoelectric transducer (see Fig. 1). Finally, i is the imaginary unit, u_s is the s-th modal coordinate and N is the number of modes (theoretically N is infinite).

The electric behaviour of the system is governed by the following expression [63]:

$$C_\infty V + \frac{V}{\mathrm{i}\omega R_0} - Q + \sum_{s=1}^{N}\theta_s u_s = 0 \tag{2}$$

where Q is the charge in one of the electrodes of the piezoelectric transducer (see Fig. 1) and R_0 is the inherent resistance of the piezoelectric transducer (that is often neglected because it is very high). Moreover, $\dot{Q}$ defines the current flowing in the circuit (i.e. the dot represents the derivative with respect to the time, see Fig. 1) and, as mentioned, C_∞ is the value of the piezoelectric capacitance at infinite frequency.

Assuming absence of external forcing (i.e. $f_e = 0$ and thus $f_{e,s} = 0$), Eq. (1) allows to derive the expression of the modal coordinate u_s as a function of the voltage V at the piezoelectric terminals:

$$u_s = \frac{\theta_s}{-\omega^2 + 2\mathrm{i}\zeta_s\omega_s\omega + \omega_s^2}V \quad \text{for} \quad s = 1,\dots,N \tag{3}$$

Substituting Eq. (3) into Eq. (2), the expression of the admittance $Y(\mathrm{i}\omega)$ of the piezoelectric transducer attached to the structure can be obtained, evidencing the contribution of the dynamics of the mechanical system:

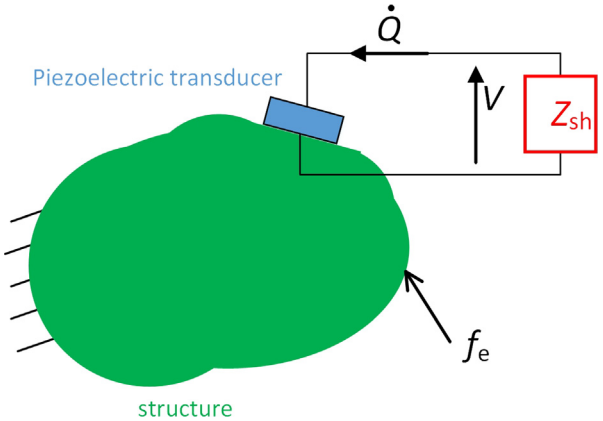

Fig. 1. Piezoelectric shunt by means of an impedance Z_{sh}.

$$Y = \frac{\dot{Q}}{V} = \frac{\mathrm{i}\omega Q}{V} = \mathrm{i}\omega\left(C_\infty + \frac{1}{\mathrm{i}\omega R_0} + \sum_{s=1}^{N} \frac{\theta_s^2}{-\omega^2 + 2\mathrm{i}\zeta_s\omega_s\omega + \omega_s^2}\right) \tag{4}$$

If only the s-th mode is taken into account, thus considering a single-degree-of-freedom (SDOF) approximation, the modal sum in Eq. (4) can be expressed as the sum of three terms: one due to the considered mode and other two accounting for the residual contributions of the neglected modes (i.e. higher and lower). Therefore, in the frequency range around ω_s (i.e. for $\omega \simeq \omega_s$), it is possible to approximate the capacitance of the piezoelectric transducer as a function of the frequency, $C(\omega)$, with the following expression:

$$C = \frac{B}{\omega} = \frac{\mathrm{Im}\{Y\}}{\omega} = \mathrm{Im}\left\{\mathrm{i}\left(C_\infty + \frac{1}{\mathrm{i}\omega R_0} + \frac{1}{-\omega^2 L_s'} + \frac{\theta_s^2}{-\omega^2 + 2\mathrm{i}\zeta_s\omega_s\omega + \omega_s^2} + C_s'\right)\right\} \tag{5}$$

where $\mathrm{Im}\{\}$ indicates the imaginary part of a complex quantity, $B(\omega) = \mathrm{Im}\{Y(\mathrm{i}\omega)\}$ is the susceptance of the piezoelectric transducer attached to the structure and L_s' and C_s' are constants accounting for the contribution of the modes lower and higher than the s-th, respectively:

$$\sum_{n=1}^{s-1} \frac{\theta_n^2}{-\omega^2 + 2\mathrm{i}\zeta_n\omega_n\omega + \omega_n^2} \simeq \sum_{n=1}^{s-1} \frac{\theta_n^2}{-\omega^2} = \frac{1}{-\omega^2 L_s'} \tag{6}$$

$$\sum_{n=s+1}^{N} \frac{\theta_n^2}{-\omega^2 + 2\mathrm{i}\zeta_n\omega_n\omega + \omega_n^2} \simeq \sum_{n=s+1}^{N} \frac{\theta_n^2}{\omega_n^2} = C_s' \tag{7}$$

The letters used to indicate the contributions from the out-of-band modes are related to the equivalent effect of the two terms on the admittance of the piezoelectric transducer attached to the structure (see Eq. (4)). Indeed, C_s' has the units of a capacitance and translates into an additional contribution to C_∞, while L_s' has the units of an inductance and, thus, shows that the modes lower than the s-th provide an inductive contribution to the behaviour of the electrical part of the whole system around ω_s. It follows that the piezoelectric capacitance $C(\omega)$ can be expressed as:

$$C = C_s + \frac{1}{-\omega^2 L_s'} + \mathrm{Re}\left\{\frac{\theta_s^2}{-\omega^2 + 2\mathrm{i}\zeta_s\omega_s\omega + \omega_s^2}\right\} = C_s + \frac{1}{-\omega^2 L_s'} + \frac{\theta_s^2\left(-\omega^2 + \omega_s^2\right)}{\left(-\omega^2 + \omega_s^2\right)^2 + \left(2\zeta_s\omega_s\omega\right)^2} \tag{8}$$

where $\mathrm{Re}\{\}$ indicates the real part of a complex quantity.

The term C_s in Eq. (8) represents the modal capacitance and is the sum of C_∞ and C_s'. In order to estimate C_s, the admittance $Y(\mathrm{i}\omega)$ of the piezoelectric transducer attached to the structure can be measured as a function of ω by means of an impedance analyzer. Then, the experimental curve describing $C(\omega)$ can be obtained from the admittance $Y(\mathrm{i}\omega)$ or the susceptance as:

$$C(\omega) = \frac{B}{\omega} = \frac{\mathrm{Im}\{Y\}}{\omega} \tag{9}$$

It is then possible to estimate the unknowns C_s and L_s' by fitting the model in Eq. (8) to the experimental curve of $C(\omega)$ obtained by measuring $Y(\mathrm{i}\omega)$ and employing Eq. (9). The values of ω_s and ζ_s are considered known in Eq. (8) because they can be estimated by modal analysis. Considering θ_s^2 in Eq. (8), in case of low modal superimposition, it can be expressed as a function of the modal electro-mechanical coupling factor k_s. Indeed, the relation between k_s and θ_s is [60]:

$$\theta_s^2 = k_s^2\omega_s^2 C_s \tag{10}$$

The modal electro-mechanical coupling factor k_s can be approximated by estimating the short- (i.e. ω_s) and open-circuit (i.e. $\hat{\omega}_s$) eigenfrequencies of the system as:

$$k_s^2 = \frac{\hat{\omega}_s^2 - \omega_s^2}{\omega_s^2} \tag{11}$$

Therefore, θ_s^2 can be approximated as (combine Eqs. (11) and (10)):

$$\theta_s^2 = C_s\left(\hat{\omega}_s^2 - \omega_s^2\right) \tag{12}$$

Eq. (12) shows that θ_s^2 can be approximated as the product of the known quantity $\left(\hat{\omega}_s^2 - \omega_s^2\right)$ (indeed, also $\hat{\omega}_s$ can be estimated by means of a modal analysis of the system) and C_s which is, together with L_s', the unknown in Eq. (8). However, θ_s^2 can also be considered as an unknown and found by means of the minimisation, together with C_s and L_s', in order to improve the fit, correcting a possible non-accurate initial estimation of θ_s^2.

This procedure employed to estimate the value of C_s and based on the use of an impedance analyzer will be the reference method in this paper. Therefore, the two new methods for estimating the value of the modal capacitance C_s, discussed in Section 3, will then be compared to this reference procedure (in Section 5).

3. Indirect methods for estimating the modal capacitance

The two methods presented here require to connect a shunt impedance Z_{sh} to the piezoelectric transducer (see Fig. 1). The possibility to identify system parameters by connecting a known impedance to the piezoelectric transducer was sketched in [39]. Here, this approach is applied to the modal capacitance and is developed and investigated. The first method requires that Z_{sh} is an inductance L (see Section 3.1), while Z_{sh} is a negative capacitance (NC) $-C_n$ for the second method (see Section 3.2).

3.1. Method 1: L-based estimation of the modal capacitance

When an inductance is shunted to the piezoelectric transducer (i.e. $Z_{sh} = i\omega L$), the relation between the charge and the voltage at the piezoelectric terminals can be expressed as:

$$Q = \frac{V}{L\omega^2} \tag{13}$$

By using Eq. (13) in the equations describing the electric behaviour of the system (see Eqs. (2), (6) and (7)), exploiting the SDOF approximation and neglecting R_0, the following equality is obtained:

$$V = \frac{-\theta_s L\omega^2}{C_s L\omega^2 - 1} u_s \tag{14}$$

To obtain this equation, the term related to L_s' has been neglected. Indeed, according to the literature (e.g. [60,65]), $1/L_s'$ is low enough to be neglected in case of low modal superimposition.

When substituting Eq. (14) into Eq. (1) and only considering mode s to describe the dynamics of the system in the frequency range around ω_s because of the low modal superimposition hypothesis, the FRF displacement/force relation of the electro-mechanical system can be derived (assuming $\zeta_s \simeq 0$):

$$\frac{u_s}{f_{e,s}} = \frac{C_s L\omega^2 - 1}{(-\omega^2 + \omega_s^2)(C_s L\omega^2 - 1) + \theta_s^2 L\omega^2} \tag{15}$$

As expected, since a shunt impedance composed by an inductance L is used, the FRF in Eq. (15) governs four poles and, thus, the presence of the shunt impedance produces two peaks around ω_s, at $\omega_{s,1}$ and $\omega_{s,2}$, in the FRF displacement/force of the system (e.g. [62,67]). These two eigenfrequencies can be found posing the denominator of the FRF in Eq. (15) equal to zero:

$$\omega^4 C_s L - \omega^2 \left[L(\theta_s^2 + C_s\omega_s^2) + 1\right] + \omega_s^2 = 0 \tag{16}$$

Solving Eq. (16), the analytical expressions of $\omega_{s,1}$ and $\omega_{s,2}$ can be found and the following equality can be obtained:

$$\omega_{s,1}^2 \omega_{s,2}^2 = \frac{\omega_s^2}{C_s L} \tag{17}$$

If $\omega_{s,1}$ and $\omega_{s,2}$ are estimated experimentally, Eq. (17) can be used to find C_s. The use of Eq. (17) is advantageous compared to the use of a single solution of Eq. (16) (i.e. either $\omega_{s,1}$ or $\omega_{s,2}$) because it allows to estimate C_s without estimating θ_s, and thus with a consequent decrease in the uncertainty associated to the estimate of C_s.It is also noticed that the basic idea of Eq. (17) is to identify some features of a primary structure by observing how the coupling to a known system changes its dynamic behaviour. This is an approach successfully adopted in other applications and with different targets (e.g. modal mass estimation [68]).

To summarise, the following steps are necessary to estimate C_s with the L-based method:

- Measure the system FRF with the piezoelectric transducer terminals short-circuited and estimate ω_s with an experimental modal analysis.
- Build an inductance L and measure/estimate its value. In theory, it could have any value. However, it is good practice to choose a value that allows to have two clear peaks for the shunted system FRF $u_s/f_{e,s}$. Such a behaviour is obtained when the inductance is tuned on the considered mode [26] and, thus, when its value is approximately:

$$L = \frac{1}{C_s\omega_s^2} \tag{18}$$

This would require to have a rough estimation of C_s in advance. However, since a fine tuning is not necessary for the procedure (i.e. just the presence of two clear peaks in the FRF is required), the first trial for the inductance value can be

obtained by using Eq. (18) with the capacitance C_{piezo} of the piezoelectric patch commonly reported on the data-sheet from the manufacturer.
- Connect the inductance to the piezoelectric transducer.
- Evaluate the system FRF $u_s/f_{e,s}$ around ω_s. If the experimental FRF does not show two clear peaks around ω_s, the value of L can be changed with a trial and error procedure until they are evident. It is important to measure/estimate the final value of L used before performing the next point on the list.
- Estimate $\omega_{s,1}$ and $\omega_{s,2}$ by experimental modal analysis on the measured FRF.
- Use Eq. (17) to find C_s.

3.2. Method 2: NC-based estimation of the modal capacitance

A shunt impedance composed by an NC, $-C_n$, is used in this case. The use of an NC allows to define a new enhanced transducer composed by the piezoelectric transducer and the NC, as evidenced in Fig. 2. The figure also shows that there are two possible connection layouts: series (see Fig. 2a) and parallel (see Fig. 2b). The capability of the NC to shift either the short- or open-circuit eigenfrequencies of the system is exploited here to estimate the modal capacitance.

Consider an electro-mechanical system with short-circuit eigenfrequencies equal to ω_s and open-circuit eigenfrequencies equal to [60] (see also Eqs. (11) and (10)):

$$\hat{\omega}_s = \sqrt{\omega_s^2 + \frac{\theta_s^2}{C_s}} \tag{19}$$

When an NC connected in series is used (see Fig. 2a), it shifts the short-circuit eigenfrequencies (i.e. short-circuiting the terminals T1 and T2 of the new enhanced transducer in Fig. 2a) towards lower frequency values [60]. The new values of the short-circuit eigenfrequencies are denoted here as ω_s^{sc}. Conversely, NCs connected in parallel (see Fig. 2b) shift the open-circuit eigenfrequencies (i.e. with the terminals T1 and T2 of the new enhanced transducer in Fig. 2b open-circuited) towards higher frequency values [60]. The new values of the open-circuit eigenfrequencies are denoted here as ω_s^{oc}. It is also noticed that the two types of connection (series/parallel) require different values of the NC, as explained below.

According to [60], for an NC in series, the value of C_n must be set higher than the value of the piezoelectric capacitance at the null frequency C_0 to assure system stability (thus, the following inequalities hold $C_n > C_0 > C_s$). In this case, for low modal superimposition, the value of ω_s^{sc} can be expressed as:

$$\omega_s^{sc} = \omega_s \sqrt{1 - \frac{\theta_s^2}{\omega_s^2 (C_n - C_s)}} \tag{20}$$

If the value of the NC used is known, as well as the short- and open-circuit eigenfrequencies (i.e. ω_s, $\hat{\omega}_s$ and ω_s^{sc}), it is possible to estimate the modal capacitance C_s combining Eqs. (20) and (19), without the need of estimating θ_s:

$$C_s = \frac{\omega_s^2 - (\omega_s^{sc})^2}{\hat{\omega}_s^2 - (\omega_s^{sc})^2} C_n \tag{21}$$

For an NC in parallel, the value of C_n must be set lower than C_∞ to assure system stability (thus, the following inequalities hold $C_n < C_\infty < C_s$), and the value of ω_s^{oc} is described by the following relation [60]:

$$\omega_s^{oc} = \omega_s \sqrt{1 + \frac{\theta_s^2}{\omega_s^2 (C_s - C_n)}} \tag{22}$$

The estimate of C_s in this case can be obtained by combining Eqs. (22) and (19):

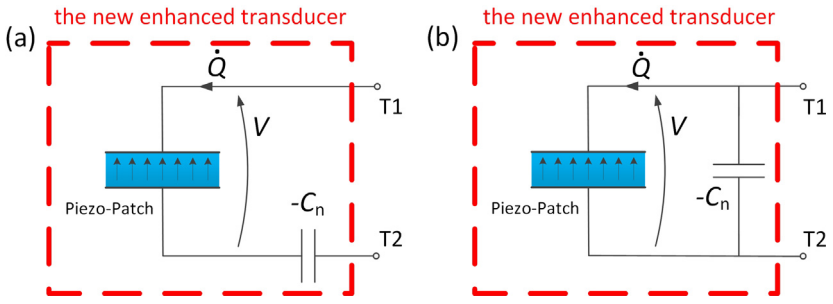

Fig. 2. A piezoelectric transducer connected to an NC in series (a) and in parallel (b). The red dashed line indicates the new enhanced transducer composed by the piezoelectric transducer and the NC.

$$C_s = \frac{\left(\omega_s^{oc}\right)^2 - \omega_s^2}{\left(\omega_s^{oc}\right)^2 - \hat{\omega}_s^2} C_n \tag{23}$$

Therefore, the following procedure can be employed in order to estimate C_s:

- Measure the system FRF with the piezoelectric terminals short- and open-circuited and estimate ω_s and $\hat{\omega}_s$, respectively, with an experimental modal analysis.
- Build an NC $-C_n$ and measure/estimate its value. The NC must assure the stability of the system and, thus, a rough estimation of either C_0 or C_∞ is needed in advance. Such an estimation can be obtained by using the capacitance of the piezoelectric patch reported on the data-sheet of the manufacturer, C_{piezo}. Then, in case the system in unstable connecting the NC to the piezoelectric transducer, the value of the NC must be adjusted until stability is reached. It is important to measure/estimate the final value of C_n used before performing the next point on the list.
- Connect the NC to the piezoelectric transducer and evaluate the system FRF.
- Estimate either ω_s^{sc} or ω_s^{oc}, according to the type of connection of the NC used, by experimental modal analysis.
- Use either Eq. (21) or Eq. (23) to find C_s.

An advantage of this procedure is that it allows to estimate C_s for different modes at the same time, with a single value of the NC (i.e. the NC affects all the modes of the electro-mechanical system), while the L-based method allows to estimate C_s only for the mode on which L is tuned.

The two methods for estimating the value of C_s described in this subsection and in Section 3.1 will be compared to the traditional fitting procedure (see Section 2) in Section 5. The next section shows how it is possible to estimate also θ_s and k_s from the methods used for estimating C_s.

4. Indirect methods for estimating the coupling coefficients

When the value of θ_s needs to be estimated, usually, Eq. (12) is used (which requires to have estimated C_s in advance) or θ_s is added among the unknowns in the fitting procedure described in Section 2. However, when a double check on the estimated θ_s value is recommended, the two methods presented in Sections 3.1 and 3.2 to estimate C_s can be employed since they provide different approaches for estimating θ_s, as explained in Section 4.1. Furthermore, the L-based method (Section 3.1) also allows for a further estimation of k_s (which is usually estimated with Eq. (11)). This additional method allows to decrease the uncertainty associated to the traditional estimation as shown in Section 4.2.

4.1. Indirect methods for estimating θ_s

When the piezoelectric transducer is shunted with an inductance L (see Section 3.1), the following relation between $\omega_{s,1}$ and $\omega_{s,2}$ can be derived from Eq. (16):

$$\omega_{s,1}^2 + \omega_{s,2}^2 = \omega_s^2 + \frac{\theta_s^2}{C_s} + \frac{1}{C_s L} \tag{24}$$

If the L-based method is used to estimate C_s, the only unknown in Eq. (24) is θ_s that can be, then, easily estimated. This θ_s estimate can be used, if needed, to check and verify the value coming from different estimation techniques. Indeed, it is noticed that the estimate of θ_s through Eq. (24) relies on the knowledge of parameters different from those on which Eq. (12) (or the fitting procedure) is based. Therefore, the procedures lead to different estimates of θ_s that can be, thus, compared.

Considering the NC-based method, the value of θ_s can be estimated using the expression of either ω_s^{sc} (Eq. (20)) or ω_s^{oc} (Eq. (22)), depending on the NC layout employed. Indeed, if C_s is estimated with the method described in Section 3.2, θ_s is the only unknown in Eqs. (20) and (22). Also in this case, the estimate of θ_s is obtained using parameters and expressions different from those traditionally employed (e.g. Eq. (12)). Therefore, the obtained θ_s values can be compared.

4.2. Indirect method for estimating k_s

This subsection shows a new method to estimate k_s relying on the connection between the piezoelectric transducer and an inductance L. Indeed, by substitution of Eqs. (17) and (10) into Eq. (24), the modal electro-mechanical coupling factor can be expressed as a function of $\omega_{s,1}, \omega_{s,2}$ and ω_s [67]:

$$k_s^2 = \frac{\omega_{s,1}^2 + \omega_{s,2}^2}{\omega_s^2} - \frac{\omega_{s,1}^2 \omega_{s,2}^2}{\omega_s^4} - 1 \tag{25}$$

This formulation reduces to $k_s^2 = \left[\left(\omega_{s,1}^2 + \omega_{s,2}^2\right)/\omega_s^2\right] - 2$ in case $L = L^{ref}$, where L^{ref} denotes the value of the inductance in Eq. (18) (see Eqs. (17) and (18)). A first advantage of the formulation of Eq. (25) is that the estimate of k_s depends on ω_s and on the eigenfrequencies generated by the inductive shunt. Indeed, $\omega_{s,1}$ and $\omega_{s,2}$ are well separated and their distance is

greater than that between ω_s and $\hat{\omega}_s$ on which the traditional estimation of k_s is based (see Eq. (11)). Therefore, in the case short- and open-circuit eigenfrequencies are really close each other and difficult to be identified with a good accuracy (e.g. low coupling factor, low frequency), this new method allows to overcome the problem since it is based on the identification of eigenfrequencies more distant from each other.

Another advantage is related to the uncertainty associated to the coupling factor estimate. Indeed, estimating k_s with Eq. (25) provides a result with a reduced uncertainty compared to the case of using Eq. (11).

The standard uncertainty v of k_s^2 can be described by means of the combined uncertainty formulation [69], which is based on a Taylor expansion. This formulation requires an estimation of the uncertainty related to the estimation of the eigenfrequencies involved in the definition of k_s^2 (either Eq. (25) or Eq. (11)). Here, the estimations of the input quantities $\omega_s, \hat{\omega}_s, \omega_{s,1}$ and $\omega_{s,2}$ are assumed as independent and the standard uncertainty associated to the estimates (evaluated by means of modal analysis) is assumed equal and here referred to as r. Assuming that the Taylor expansion can be truncated to the first order terms for the sake of simplicity, v assumes the following expression when k_s^2 is estimated with Eq. (11):

$$v = \sqrt{\left(\frac{\partial k_s^2}{\partial \omega_s} r\right)^2 + \left(\frac{\partial k_s^2}{\partial \hat{\omega}_s} r\right)^2} = 2r \frac{\hat{\omega}_s}{\omega_s^2} \sqrt{1 + \frac{\hat{\omega}_s^2}{\omega_s^2}} \tag{26}$$

Conversely, when k_s^2 is estimated with Eq. (25), v is:

$$\begin{aligned} v &= \sqrt{\left(\frac{\partial k_s^2}{\partial \omega_s} r\right)^2 + \left(\frac{\partial k_s^2}{\partial \omega_{s,1}} r\right)^2 + \left(\frac{\partial k_s^2}{\partial \omega_{s,2}} r\right)^2} \\ &= 2r \frac{1}{\omega_s^5} \sqrt{4\omega_{s,1}^4 \omega_{s,2}^4 + \omega_s^2 \left(\omega_{s,1}^2 + \omega_{s,2}^2\right)\left(\omega_s^4 - 3\omega_{s,1}^2 \omega_{s,2}^2\right) + \omega_s^4 \left(\omega_{s,1}^2 - \omega_{s,2}^2\right)^2} \end{aligned} \tag{27}$$

From here on, v is denoted as v_{cl} for the classical estimation method (see Eq. 26) and as v_{L} for the newly proposed method (see Eq. 27). The two uncertainties can be compared by calculating the ratio $v_{\mathrm{L}}/v_{\mathrm{cl}}$ as a function of two parameters: k_s, which governs the distance between ω_s and $\hat{\omega}_s$, and L which affects the distance between $\omega_{s,1}$ and $\omega_{s,2}$. This analysis is shown in Fig. 3a where the different curves are related to different L values. The values of L are expressed as referenced to the L value of Eq. (18), denoted as L^{ref} in the figure. Looking at Fig. 3a, it can be seen that the influence of the L value is to modify the value

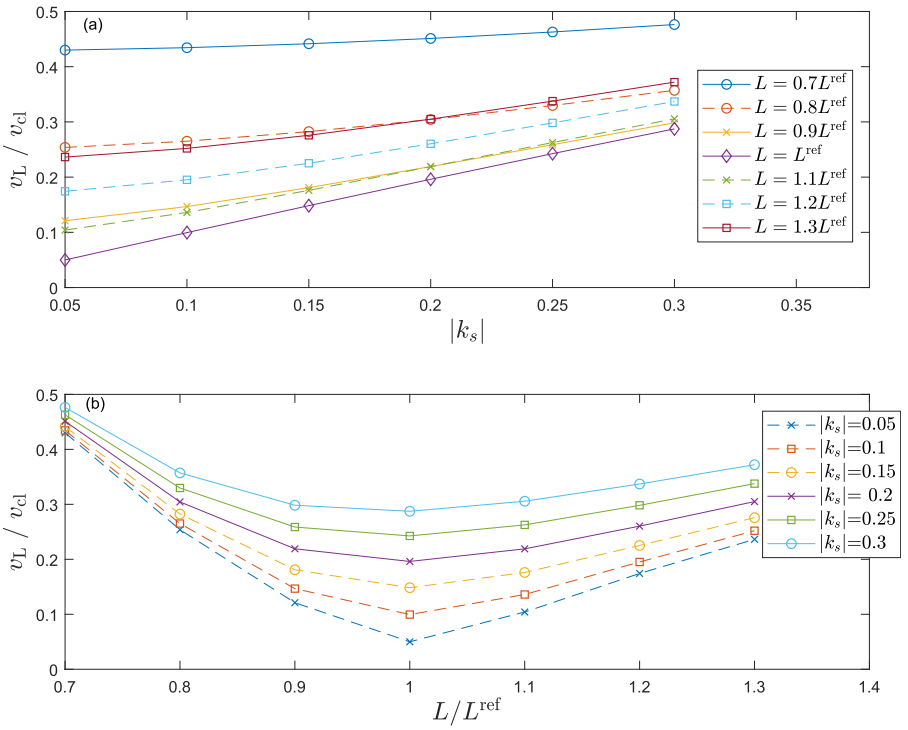

Fig. 3. The trend of $v_{\mathrm{L}}/v_{\mathrm{cl}}$ as a function of the $|k_s|$ value for different L values (a) and as a function of the ratio L/L^{ref} for different $|k_s|$ values. Here, $\zeta_s = 5 \times 10^{-4}$ and C_s = 39 nF (this value was chosen in order to stay close to the C_s values of the system used for the experiments in Section 5).

of v_L because of the change of the values and relative distances of the eigenfrequencies $\omega_{s,1}$ and $\omega_{s,2}$. However, regardless the value of the inductance used, and despite that the ratio v_L/v_{cl} increases with k_s, it is evident that v_L is always significantly lower than v_{cl}.

In order to clarify the influence of the value of L on v_L, it is noticed that this relationship is not straightforward to be analysed because v_L depends on both the distance between $\omega_{s,1}$ and $\omega_{s,2}$ and on their absolute values (see Eq. (27)). Therefore, when L is changed, there are two effects to be considered and they can have an opposite influence on the resulting value of v_L. However, Fig. 3b allows to achieve a clear conclusion about which L value is the one allowing to reduce v_L as much as possible. In this figure, the trend of v_L/v_{cl} is depicted as a function of the ratio L/L^{ref} for systems with different $|k_s|$ values. In all the cases, the value of L equal to L^{ref} is always able to reduce as much as possible v_L.

The next section describes the experimental tests carried out to validate the methods presented in this subsection and in Section 3.

5. Experimental validation of the methods

This section presents the tests carried out to validate the L-based and NC-based methods for estimating the modal capacitance and also the method presented in Section 4.2 for the estimation of $|k_s|$. At first, the set-up is described in Section 5.1 and then the results of the tests are presented in Section 5.2.

5.1. The experimental set-up

The set-up used was a stainless steel cantilever beam (length of about 18 cm, width of approximately 3 cm and thickness of about 1 mm) with two piezoelectric patches (length 70 mm, width 30.0 mm, thickness 0.55 mm, material PIC 151) bonded at the clamped end (one per side) and electrically connected in series (see Fig. 4). The beam was forced by using a contactless actuator composed of a coil and a magnet bonded close to the tip (the force exerted to the beam was assumed as proportional to the measured current flowing through the coil [70]), while the structural response was measured by means of a laser velocimeter. The measured FRFs velocity/force allowed to find the FRFs displacement/force just by diving them with $i\omega$.

Considering the L-based method for the estimation of C_s and $|k_s|$, the tests were carried out on the first bending mode of the beam. The main reason for choosing the first mode of the beam was to have an eigenfrequency with a low value (approximately 32 Hz) and thus a high value for L (e.g. see Eq. (18)). In this way, it was possible to demonstrate the practical feasibility of the L-based method also in a disadvantageous situation. Indeed, since the value required for L was high, a synthetic inductor was built by using the Antoniou's circuit [26,71] based on operational amplifiers. The circuit is shown in Fig. 5a. Here, the variable resistance R_{p1} was used in order to produce a negative resistance in series with L. This negative resistance was needed to eliminate parasitic resistances that can be present when using operational amplifiers to simulate inductances. The total residual resistance was estimated to 500 Ω, that was considered a value low enough not to affect the experimental tests (also according to simulations).

For the NC-based method, the NC was connected in series in order to work on the first bending modes of the beam [60]. The circuit used was that of Fig. 5b. It can be modelled as the parallel connection of an NC and a negative resistance. The value of R_{comp} was chosen in order to make the resistance highly negative (i.e. -75 MΩ). This allows the circuit of Fig. 5b to behave like a pure NC. More details about this circuit can be found in [60].

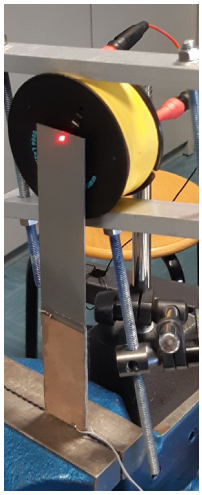

Fig. 4. The set-up.

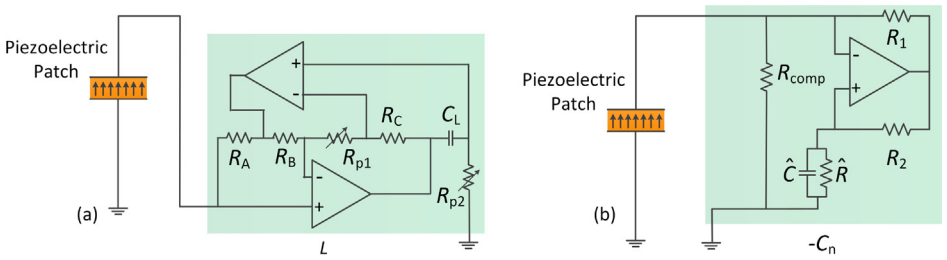

Fig. 5. The electrical schematics used to build the shunt inductance for the *L*-based method (a) and the NC shunt for the NC-based method (b).

The values used for the components of the circuits of Fig. 5 are provided in Table 1. All the operational amplifiers used were of type OPA445 and were supplied with a voltage of ±30 V.

Considering the tests with the reference method for estimating C_s described in Section 2 (i.e. the fitting procedure), they were performed with an impedance analyzer.

Finally, the modal parameters (e.g. eigenfrequencies) which are needed for using the methods proposed in this paper were identified via modal analysis by means of a least-squares complex-frequency domain method (e.g. [72]).

5.2. Tests

At first, the tests related to the estimation of C_s are discussed here. These tests lasted an entire day. The measurement with the impedance analyzer was repeated three times during the day (before the tests with the *L*-based method, between the tests with *L*-based and NC-based methods, and after all tests had been conducted). Therefore, the effect of the temperature change, that inherently occurred during the day in the lab, on the value of the modal capacitance is present in the results of the reference method. This was unavoidable because the tests for both the *L*-based and NC-based methods lasted some hours and could not be performed at the same nominal temperature (the temperature in the room of the tests can change of few Kelvin during the day). Together with the tests using the impedance analyzer, also tests forcing the structure were performed continuously in order to estimate each time the values of ω_s, ζ_s and $\hat{\omega}_s$. Their values for one of these tests are reported in Table 2.

The tests with the *L*-based approach were carried out with six different values of *L* (gathered in Table 3). This allowed to check the dispersion of the results of the method. Seven tests were carried out for the NC-based method, with seven different values of the NC (see Table 3). Since the aim of the new proposed methods is to have an inexpensive approach for estimating C_s, the values of *L* and C_n were not measured (this would require a device able to characterise an active element), but theoretical formulas were instead employed directly to estimate the *L* and C_n values. This allows to test both the methods without the use of any additional device. More precisely, *L* was estimated as (refer to the elements in Fig. 5a):

$$L = \frac{C_L R_A R_C R_{p2}}{R_B} \tag{28}$$

and C_n was estimated as (refer to the elements in Fig. 5b):

$$C_n = \frac{R_2}{R_1}\hat{C} \tag{29}$$

The resistances and capacitances in Eqs. (28) and (29) were measured with an inexpensive basic multimeter.

Figs. 6a, b and c show the fit of the capacitance of the piezoelectric patch with the model of Eq. (8) (setting C_s, L_s' and θ_s as the unknowns to be found) around the third bending mode of the beam for one of the tests with the impedance analyzer (a), the system FRF showing the influence of the additional *L* in method 1 (b), and the system FRF with the shift of the short-circuit eigenfrequency due to the NC in series in method 2 (c), respectively.

Fig. 7 shows the C_s results of the different methods for the first three bending modes of the beam (obviously, the results for the *L*-based method are absent for the second and third mode). There is a good superimposition among the different results for the first mode and the reproducibility of the different methods is comparable (see the magnification in Fig. 8a). In the case of the third mode, again, the results are more than satisfactory (see the magnification in Fig. 8b). Conversely, for the second mode, there is a bias between the results of the reference method and of the NC-based method

Table 1
Values of the components of the circuits in Fig. 5.

R_A [kΩ]	R_B [kΩ]	R_C [kΩ]	C_L [μF]	R_{p2}	R_1	R_2 [kΩ]	$\hat{R}$	R_{comp} [MΩ]	$\hat{C}$ [nF]
1.98	0.99	0.99	4.84	Variable	Variable	11.47	Variable	2.91	69.23

Table 2
Values of ω_s, ζ_s and $\hat{\omega}_s$ for one of the tests.

bending mode	$\omega_s/(2\pi)$ [Hz]	ζ_s	$\hat{\omega}_s/(2\pi)$ [Hz]
1	32.48	4.2×10^{-3}	33.40
2	154.09	7.2×10^{-3}	154.53
3	437.67	1.7×10^{-3}	440.05

Table 3
Values of L and C_n used in the tests.

	Test 1	Test 2	Test 3	Test 4	Test 5	Test 6	Test 7
L [H]	$607.9 \simeq L^{ref}$	589.7	571.4	553.2	534.9	516.7	–
C_n [nF]	112.9	87.8	79.0	71.9	65.9	60.8	56.5

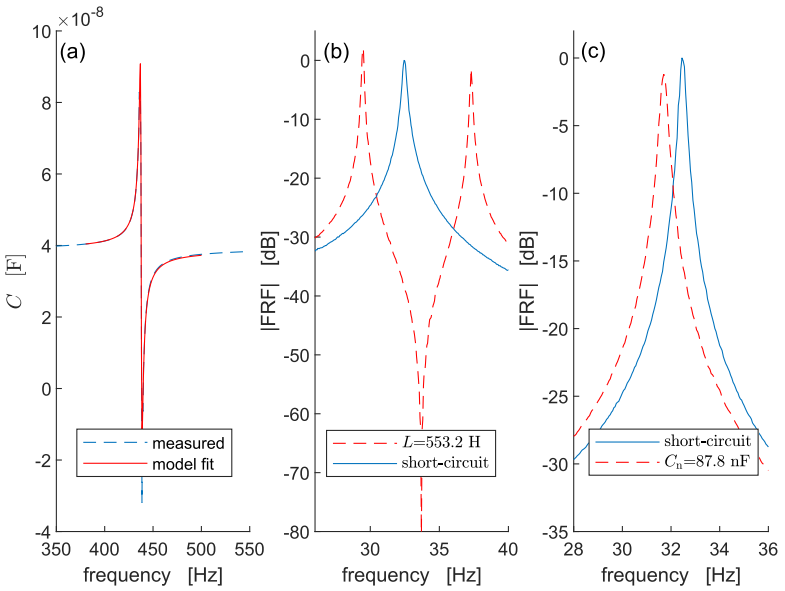

Fig. 6. Fit of the capacitance of the piezoelectric patch at the third mode for one of the tests with the impedance analyzer (a), magnitude of the measured FRFs of the system (displacement/force) at the first mode showing the effect of the addition of L in method 1 (b), and magnitude of the measured FRFs of the system (displacement/force) at the first mode showing the shift of the short-circuit eigenfrequency due to the NC in method 2 (c).

(although, the order of magnitude of the results of the two methods is the same). The reason for this discrepancy is that the first mode peak is much higher than for the second mode in the displacement/force FRF of the system (due to higher eigenmode components). This makes the hypothesis of low modal coupling (which is at the foundation of the method) not valid for $\omega \simeq \omega_2$ with a non-negligible influence from the first mode. Therefore, to face situations like these, in which the modal superimposition is too large, a modified approach is needed. The solution is to adopt a multi-degree-of-freedom (MDOF) model to take into account the first two modes of the beam (those interesting for the problem) and the effect of the NC. Such a model, developed in [63], is briefly described in Appendix A, while in this section only the results are discussed (represented with yellow crosses in Fig. 7). The use of the MDOF model allows to improve the estimation of C_s, eliminating the previously evidenced bias. Finally, Fig. 8c shows, for the second mode, the results of the reference method superimposed to the mean value of the results of the NC-based method with the SDOF (black square) and MDOF (yellow cross) models. The solid lines show the spans between the largest and smallest results for the two types of NC-based method. This allows to stress the benefits provided in this case by the MDOF approach and to evidence the reliability of the proposed method even in case of significant modal superimposition. Obviously, in a real application, one should analyse the system FRF in order to evaluate whether the MDOF approach is needed or the SDOF one can be employed. It is also important to notice that the same MDOF approach can be used with the L-based method with similar results as those obtained for the NC-based method. Therefore, even if the L-based and NC-based methods have been initially presented under the hypothesis of low modal superimposition, the results shown above enable to evidence that they can provide reliable estimations of C_s also when this hypothesis is not fulfilled, by using the MDOF model.

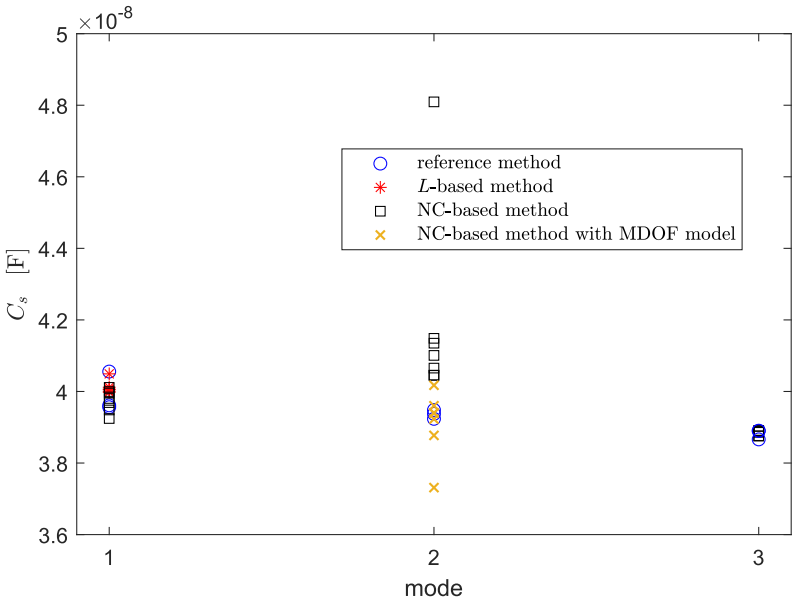

Fig. 7. Results of the *L*-based and NC-based methods compared to the reference method for the first three modes of the beam.

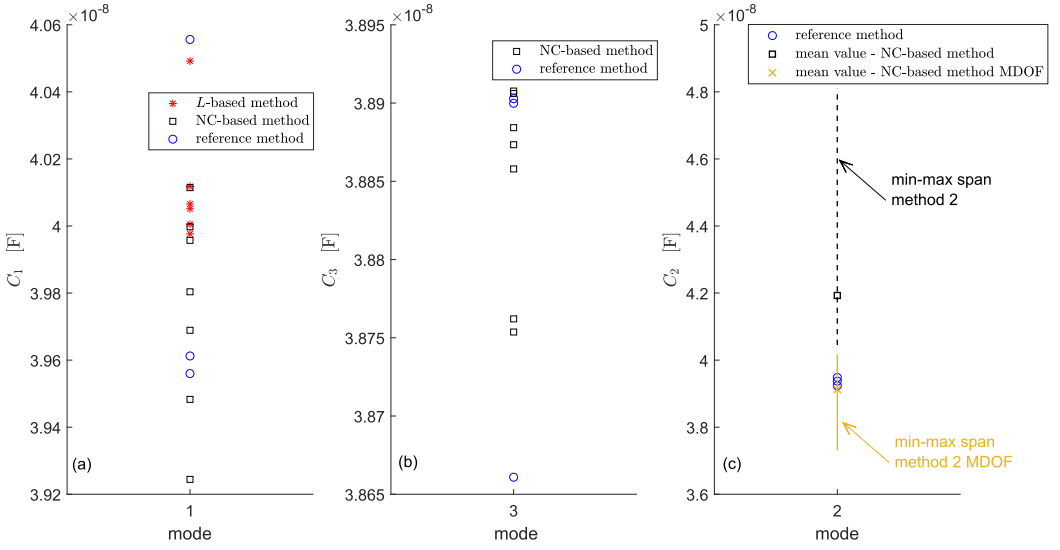

Fig. 8. Results of different methods for the first (a), third (b) and second (c) bending mode.

As a concluding remark, it is possible to suggest to always carry out more than one measurement of C_s when using either the *L*-based or the NC-based method. Indeed, the mean value of the results is expected to be a reliable estimator of the modal capacitance.

Finally, the newly proposed method to estimate $|k_s|$ (see Section 4.2) was tested on the first bending mode of the beam. To this purpose, a modal analysis was repeated five times with the piezoelectric patch in both short- and open-circuit. This allowed to estimate five values of $|k_1|$ with Eq. (11). Furthermore, also a modal analysis with the piezoelectric patch connected to an inductance like that of test 2 in Table 3 was repeated five times, allowing to obtain five values of $|k_1|$ estimated through Eq. (25). The results are shown in Fig. 9. A slight bias (i.e. different mean values) can be evidenced between the results of the two methods. This is mainly due to thermal changes during the test session of the two methods. However, this bias is so small that it can be considered negligible for practical applications. The interesting outcome of this figure is that the result dispersion related to the new method is much lower compared to the classical method, therefore implying a lower uncertainty. This is in accordance with the uncertainty analysis performed in Section 4.2 (particularly, see Fig. 3).

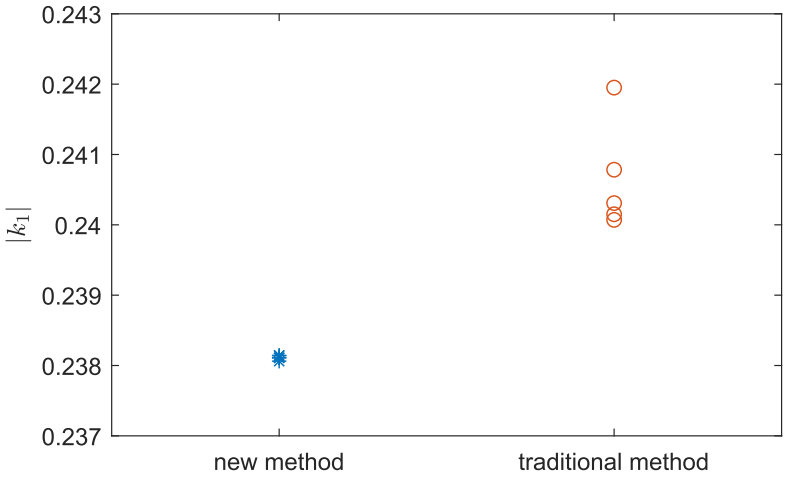

Fig. 9. The estimation of $|k_1|$ with the classical experimental approach (see Eq. (11)) and the newly proposed one related to the connection of the piezoelectric patch to an inductance (see Eq. (25)).

6. Conclusion

This paper has described two indirect methods for estimating the value of the modal capacitance for piezoelectric transducers using vibration measurements and low-cost electronic devices, thus avoiding the measurement of electrical voltage and current. This results in an inexpensive experimental set-up. One method requires to connect the piezoelectric transducer to an inductance L, while the other to an NC. Furthermore, the L-based method also allows for an estimation of the modal electro-mechanical coupling factor affected by less uncertainty compared to what occurs for the usual experimental estimation approach.

Considering the estimation of the modal capacitance, both methods have been validated against one of the reference methods available in the literature, showing satisfactory performances. Indeed, the results have been in accordance with those provided by the reference method and also the result dispersion was comparable. The paper has also shown that it is possible to successfully estimate the modal capacitance even when the modal superimposition is significant. This is possible by using an MDOF model for the NC-based method (a similar approach is possible also for the L-based method).

Considering the estimation of the modal electro-mechanical coupling factor, the experimental results proved the capability of the L-based method to provide estimations of $|k_s|$ with lower uncertainty than the classical experimental method commonly used to estimate it.

Declaration of Competing Interest

The authors declare that they have no known competing financial interests or personal relationships that could have appeared to influence the work reported in this paper.

Acknowledgment

This research has financially been supported at University of Parma by the Programme “FIL-Quota Incentivante” of University of Parma and co-sponsored by Fondazione Cariparma. Furthermore, the Italian Ministry of Education, University and Research is acknowledged by S. Manzoni (Politecnico di Milano) for the support provided through the Project “Department of Excellence LIS4.0 – Lightweight and Smart Structures for Industry 4.0”.

Appendix A. The MDOF model

This appendix briefly recalls the basics of the MDOF model presented in [63]. The system with the open-circuited piezoelectric transducer is represented by means of a state space model. The matrices of this model depend on the modal parameters of the structure (i.e. eigenfrequencies and eigenvector components scaled to the unit modal mass, with the short-circuited piezoelectric transducer, and associated non-dimensional damping ratios for the first two bending modes of the system, i.e. $s = 1, 2$) that can be estimated by means of modal analysis. In this specific case, the matrices depend on three further variables:

1. θ_1: it can be estimated finding C_1 with the NC-based method (see Section 3.2) and then inserting this C_1 value into Eq. (12). It is recalled that C_1 can be directly estimated with the method of Section 3.2 because the corresponding mode is not severely influenced by the surrounding modes.
2. C_2: it is the unknown of the problem.
3. θ_2: it can be expressed as a function of the unknown C_2 by using Eq. (12).

The expressions of the matrices are as follows:

$$\mathbf{A} = \begin{bmatrix} -2\omega_1\zeta_1 & -\omega_1^2\left[1+\theta_1^2/(\omega_1^2 C_2)\right] & 0 & -(\theta_1\theta_2)/C_2 & -\theta_1/(R_0 C_2\sqrt{C_2}) \\ 1 & 0 & 0 & 0 & 0 \\ 0 & -(\theta_1\theta_2)/C_2 & -2\omega_2\zeta_2 & -\omega_2^2\left[1+\theta_2^2/(\omega_2^2 C_2)\right] & -\theta_2/(R_0 C_2\sqrt{C_2}) \\ 0 & 0 & 1 & 0 & 0 \\ 0 & -\theta_1/\sqrt{C_2} & 0 & -\theta_2/\sqrt{C_2} & -1/(R_0 C_2) \end{bmatrix} \tag{A.1}$$

$$\mathbf{B}_\mathrm{f}^\mathrm{T} = \begin{bmatrix} \phi_1(x_\mathrm{f}) & 0 & \phi_2(x_\mathrm{f}) & 0 & 0 \end{bmatrix} \tag{A.2}$$

$$\mathbf{B}_\mathrm{w}^\mathrm{T} = \begin{bmatrix} \theta_1/\sqrt{C_2} & 0 & \theta_2/\sqrt{C_2} & 0 & 1 \end{bmatrix} \tag{A.3}$$

$$\mathbf{C}_\mathrm{z} = \begin{bmatrix} 0 & \phi_1(x_\mathrm{m}) & 0 & \phi_2(x_\mathrm{m}) & 0 \end{bmatrix} \tag{A.4}$$

$$\mathbf{C}_\mathrm{y} = \begin{bmatrix} 0 & 0 & 0 & 0 & -1 \end{bmatrix} \tag{A.5}$$

in which $\phi_s(\mathrm{x_f})$ and $\phi_s(\mathrm{x_m})$ are the eigenvector components (scaled to the unit modal mass and with the piezoelectric transducer short-circuited) of mode s at locations x_f (i.e. where the disturbance f_e is applied) and x_m (i.e. where the system response is collected), respectively, with the superscript T indicating the matrix transpose.

These matrices form the following state space description of the electro-mechanical system:

$$\begin{cases} \dot{\mathbf{g}} = \mathbf{A}\mathbf{g} + \mathbf{B}_\mathrm{w}\overline{Q} + \mathbf{B}_\mathrm{f} f_\mathrm{e} \\ w(x_\mathrm{m}) = \mathbf{C}_\mathrm{z}\mathbf{g} \\ y = \mathbf{C}_\mathrm{y}\mathbf{g} \end{cases} \tag{A.6}$$

where $w(x_\mathrm{m})$ is the displacement of the system in x_m, y is the output of the system, $\overline{Q} = Q/\sqrt{C_2}$ and $\mathbf{g}$ is the vector containing the state variables:

$$\mathbf{g}^\mathrm{T} = \begin{bmatrix} \dot{u}_1 & u_1 & \dot{u}_2 & u_2 & \int\overline{V} \end{bmatrix} \tag{A.7}$$

where the symbol $\int\overline{V}$ is used to indicate the integral with respect to the time of $\overline{V}$, with $\overline{V} = V\sqrt{C_2}$.

The effect of the shunt impedance in this model is that of a controller which acts via a feedback loop. Therefore, in this case where the shunt impedance is an NC, the system results controlled by means of a controller which depends on the values of C_n and C_2. The transfer function K_nc of the controller in the Laplace domain (the Laplace operator is defined here as S) is:

$$K_\mathrm{nc} = \frac{\overline{Q}}{y}(S) = \frac{-C_\mathrm{n}S}{C_2} \tag{A.8}$$

Using the previously defined matrices and controller transfer function, the transfer function T_wf of the shunted system between f_e and $w(x_\mathrm{m})$ can be written as:

$$T_\mathrm{wf}(S) = \mathbf{C}_\mathrm{z}\left(S\mathbf{I} - \left[\mathbf{A} + \mathbf{B}_\mathrm{w}K_\mathrm{nc}\mathbf{C}_\mathrm{y}\right]\right)^{-1}\mathbf{B}_\mathrm{f} \tag{A.9}$$

where $\mathbf{I}$ is the identity matrix.

From this transfer function displacement/force, the corresponding FRF can be easily obtained. If this FRF with the shunted NC is experimentally measured, it can be used for fitting the model of the controlled system with C_2 as the only unknown to be tuned.

In case of doubt about the accuracy of the estimation of θ_1 because of closed modes (suppose to consider a system different from that tested), its initial value can be estimated by using the approach described in the first point in the previous numbered list and then it can be included in the model as a variable to be tuned through the minimisation, together with C_2.

Finally, it is noticed that the tests used to estimate θ_1 (see the first point in the previous numbered list) are the same employed to find C_2 with the fitting procedure, using the MDOF model, and no repetition of the tests is therefore needed.

A similar MDOF model can be used also when employing an inductance L to shunt the piezoelectric transducer.

References

[1] C. Fuller, S. Elliott, P. Nelson, Active Control of Vibration, Academic Press, 1997.
[2] A. Preumont, B. de Marneffe, A. Deraemaeker, F. Bossens, The damping of a truss structure with a piezoelectric transducer, Comput. Struct. 86 (3–5) (2008) 227–239, https://doi.org/10.1016/j.compstruc.2007.01.038.
[3] D. Meng, P. Xia, K. Lang, E. Smith, C. Rahn, Neural network based hysteresis compensation of piezoelectric stack actuator driven active control of helicopter vibration, Sens. Actuat. A Phys. 302 (2020) Article ID: 111809. doi: 10.1016/j.sna.2019.111809..
[4] Q. Hu, G. Ma, Variable structure control and active vibration suppression of flexible spacecraft during attitude maneuver, Aerosp. Sci. Technol. 9 (4) (2005) 307–317, https://doi.org/10.1016/j.ast.2005.02.001.
[5] M. Sabatini, G. Palmerini, P. Gasbarri, Synergetic approach in attitude control of very flexible satellites by means of thrusters and pzt devices, Aerosp. Sci. Technol. 96 (2020) Article ID: 105541. doi: 10.1016/j.ast.2019.105541..
[6] G. Song, V. Sethi, H.N. Li, Vibration control of civil structures using piezoceramic smart materials: a review, Eng. Struct. 28 (11) (2006) 1513–1524, https://doi.org/10.1016/j.engstruct.2006.02.002.
[7] P. Shivashankar, S. Gopalakrishnan, Review on the use of piezoelectric materials for active vibration, noise, and flow control, Smart Mater. Struct. 29 (5) (2020) Article ID: 053001. doi: 10.1088/1361-665X/ab7541..
[8] Y. Luo, X. Zhang, Y. Zhang, Y. Qu, M. Xu, K. Fu, L. Ye, Active vibration control of a hoop truss structure with piezoelectric bending actuators based on a fuzzy logic algorithm, Smart Mater. Struct. 27 (8) (2018) Article ID: 085030. doi: 10.1088/1361-665X/aad1b6..
[9] S. Narayanan, V. Balamurugan, Finite element modelling of piezolaminated smart structures for active vibration control with distributed sensors and actuators, J. Sound Vib. 262 (3) (2003) 529–562, https://doi.org/10.1016/S0022-460X(03)00110-X.
[10] S. Kang, H. Wu, X. Yang, Y. Li, Y. Wang, Fractional-order robust model reference adaptive control of piezo-actuated active vibration isolation systems using output feedback and multi-objective optimization algorithm, J. Vib. Control 26 (1–2) (2020) 19–35, https://doi.org/10.1177/1077546319875260.
[11] C.M. Vasques, J. Dias Rodrigues, Active vibration control of smart piezoelectric beams: comparison of classical and optimal feedback control strategies, Comput. Struct. 84 (22–23) (2006) 1402–1414, https://doi.org/10.1016/j.compstruc.2006.01.026.
[12] J. Peng, G. Zhang, M. Xiang, H. Sun, X. Wang, X. Xie, Vibration control for the nonlinear resonant response of a piezoelectric elastic beam via time-delayed feedback, Smart Mater. Struct. 28 (9) (2019) Article ID: 095010. doi: 10.1088/1361-665X/ab2e3d..
[13] J. Hu, Z. Kang, Topological design of piezoelectric actuator layer for linear quadratic regulator control of thin-shell structures under transient excitation, Smart Mater. Struct. 28 (9). doi: 10.1088/1361-665X/ab1e96..
[14] M. Moretti, E. Silva, J. Reddy, Topology optimization of flextensional piezoelectric actuators with active control law, Smart Mater. Struct. 28 (3) (2019) Article ID: 035015. doi:10.1088/1361-665X/aafd56..
[15] X. Ma, Z. Wang, B. Zhou, S. Xue, A study on performance of distributed piezoelectric composite actuators using Galerkin method, Smart Mater. Struct. 28 (10) (2019) Article ID: 105049. doi:10.1088/1361-665X/ab3f3d..
[16] A. Baz, S. Poh, Performance of an active control system with piezoelectric actuators, J. Sound Vib. 126 (2) (1988) 327–343, https://doi.org/10.1016/0022-460X(88)90245-3.
[17] I. Bruant, L. Gallimard, S. Nikoukar, Optimal piezoelectric actuator and sensor location for active vibration control, using genetic algorithm, J. Sound Vib. 329 (10) (2010) 1615–1635, https://doi.org/10.1016/j.jsv.2009.12.001.
[18] K. Ramesh Kumar, S. Narayanan, Active vibration control of beams with optimal placement of piezoelectric sensor/actuator pairs, Smart Mater. Struct. 17 (5) (2008) Article ID: 055008. doi: 10.1088/0964-1726/17/5/055008..
[19] V. Gupta, M. Sharma, N. Thakur, Optimization criteria for optimal placement of piezoelectric sensors and actuators on a smart structure: a technical review, J. Intell. Mater. Syst. Struct. 21 (12) (2010) 1227–1243, https://doi.org/10.1177/1045389X10381659.
[20] Z. Qiu, X. Zhang, H. Wu, H. Zhang, Optimal placement and active vibration control for piezoelectric smart flexible cantilever plate, J. Sound Vib. 301 (3–5) (2007) 521–543, https://doi.org/10.1016/j.jsv.2006.10.018.
[21] A. Belloli, P. Ermanni, Optimum placement of piezoelectric ceramic modules for vibration suppression of highly constrained structures, Smart Mater. Struct. 16 (5) (2007) 1662–1671, https://doi.org/10.1088/0964-1726/16/5/019.
[22] W.P. Li, H. Huang, Integrated optimization of actuator placement and vibration control for piezoelectric adaptive trusses, J. Sound Vib. 332 (1) (2013) 17–32, https://doi.org/10.1016/j.jsv.2012.08.005.
[23] D. Oshmarin, N. Iurlova, N. Sevodina, M. Iurlov, Algorithm for the layout of a piezoelectric element in an elastic medium providing the maximal piezoelectric effect within a specified frequency range, Int. J. Smart Nano Mater. 10 (4) (2019) 268–284, https://doi.org/10.1080/19475411.2019.1576070.
[24] A. Preumont, Mechatronics: Dynamics of Electromechanical and Piezoelectric Systems, Springer, 2006.
[25] S. Moheimani, A. Fleming, Piezoelectric Transducers for Vibration Control and Damping, Springer-Verlag, 2006.
[26] O. Thomas, J. Ducarne, J. Deü, Performance of piezoelectric shunts for vibration reduction, Smart Mater. Struct. 21 (1) (2012), Article ID 015008.
[27] J. Ducarne, O. Thomas, J. Deü, Placement and dimension optimization of shunted piezoelectric patches for vibration reduction, J. Sound Vib. 331 (14) (2012) 3286–3303.
[28] S. Chesne, C. Jean-Mistral, L. Gaudiller, Experimental identification of smart material coupling effects in composite structures, Smart Mater. Struct. 22 (2013) Article ID: 075007. doi:10.1088/0964-1726/22/7/075007..
[29] R. Nowak, M. Pietrzakowski, P. Rumianek, Influence of design parameters on bending piezoelectric harvester effectiveness: static approach, Mech. Syst. Signal Process. 143 (2020) Article ID: 106833. doi:10.1016/j.ymssp.2020.106833..
[30] B. Bayik, A. Aghakhani, I. Basdogan, A. Erturk, Equivalent circuit modeling of a piezo-patch energy harvester on a thin plate with ac-dc conversion, Smart Mater. Struct. 25 (5) (2016) 055015.
[31] P. Peralta, R. Ruiz, A. Taflanidis, Bayesian identification of electromechanical properties in piezoelectric energy harvesters, Mech. Syst. Signal Process. 141 (2020) Article ID: 106506. doi: 10.1016/j.ymssp.2019.106506..
[32] N. Hagood, A. von Flotow, Damping of structural vibrations with piezoelectric materials and passive electrical networks, J. Sound Vib. 146 (1991) 243–268.
[33] A. Badel, G. Sebald, D. Guyomar, M. Lallart, E. Lefeuvre, C. Richard, J. Qiu, Piezoelectric vibration control by synchronized switching on adaptive voltage sources: towards wideband semi-active damping, J. Acoust. Soc. Am. 119 (5) (2006) 2815–2825, https://doi.org/10.1121/1.2184149.
[34] R. Darleux, B. Lossouarn, J.-F. Deü, Passive self-tuning inductor for piezoelectric shunt damping considering temperature variations, J. Sound Vib. 432 (2018) 105–118.
[35] G. Caruso, A critical analysis of electric shunt circuits employed in piezoelectric passive vibration damping, Smart Mater. Struct. 10 (5) (2001) 1059–1068.
[36] G. Tairidis, Vibration control of smart composite structures using shunted piezoelectric systems and neuro-fuzzy techniques, J. Vib. Control 25 (18) (2019) 2397–2408.
[37] P. Gardonio, D. Casagrande, Shunted piezoelectric patch vibration absorber on two-dimensional thin structure: tuning considerations, J. Sound Vib. 395 (2017) 26–47.
[38] V. Matveenko, N. Iurlova, D. Oshmarin, N. Sevodina, M. Iurlov, An approach to determination of shunt circuits parameters for damping vibrations, Int. J. Smart Nano Mater. 9 (2) (2018) 135–149.
[39] U. Andreaus, M. Porfiri, Effect of electrical uncertainties on resonant piezoelectric shunting, J. Intell. Mater. Syst. Struct. 18 (2007) 477–485.
[40] J. Høgsberg, S. Krenk, Balanced calibration of resonant shunt circuits for piezoelectric vibration control, J. Intell. Mater. Syst. Struct. 23 (17) (2012) 1937–1948..

[41] J. Høgsberg, S. Krenk, Balanced calibration of resonant piezoelectric rl shunts with quasi-static background flexibility correction, J. Sound Vib. 341 (2015) 16–30..
[42] P. Soltani, G. Kerschen, G. Tondreau, A. Deraemaeker, Tuning of a piezoelectric vibration absorber attached to a damped structure, J. Intell. Mater. Syst. Struct. 28 (9) (2017) 1115–1129.
[43] K. Yamada, H. Matsuhisa, H. Utsuno, K. Sawada, Optimum tuning of series and parallel LR circuits for passive vibration suppression using piezoelectric elements, J. Sound Vib. 329 (24) (2010) 5036–5057.
[44] S.-Y. Wu, Method for multiple mode piezoelectric shunting with single PZT transducer for vibration control, J. Intell. Mater. Syst. Struct. 9 (1998) 991–998.
[45] S. Behrens, S. Moheimani, A. Fleming, Multiple mode current flowing passive piezoelectric shunt controller, J. Sound Vib. 266 (5) (2003) 929–942, https://doi.org/10.1016/S0022-460X(02)01380-9.
[46] A.J. Fleming, S. Behrens, S.O.R. Moheimani, Reducing the inductance requirements of piezoelectric shunt damping systems, Smart Mater. Struct. 12 (1) (2003) 57–64, https://doi.org/10.1088/0964-1726/12/1/307.
[47] G. Raze, A. Paknejad, G. Zhao, C. Collette, G. Kerschen, Multimodal vibration damping using a simplified current blocking shunt circuit, J. Intell. Mater. Syst. Struct. in press. doi: 10.1177/1045389X20930103..
[48] S. Behrens, A.J. Fleming, S.O.R. Moheimani, A broadband controller for shunt piezoelectric damping of structural vibration, Smart Mater. Struct. 12 (1) (2003) 18–28.
[49] B.S. Beck, K.A. Cunefare, M. Collet, The power output and efficiency of a negative capacitance shunt for vibration control of a flexural system, Smart Mater. Struct. 22 (6), Article ID: 065009..
[50] G. Raze, B. Lossouarn, A. Paknejad, G. Zhao, J.-F. Deü, C. Collette, G. Kerschen, A multimodal nonlinear piezoelectric vibration absorber, in: Proceedings of the International Conference on Noise and Vibration Engineering ISMA and International Conference on Uncertainty in Structural Dynamics USD – September 17–19, 2018 – Leuven (Belgium), 2018.
[51] G. Raze, A. Jadoul, S. Guichaux, V. Broun, G. Kerschen, A digital nonlinear piezoelectric tuned vibration absorber, Smart Mater. Struct. 29 (1) (2020) Article ID: 015007. doi:10.1088/1361-665X/ab5176..
[52] C. Bricault, C. Pézerat, M. Collet, A. Pyskir, P. Perrard, G. Matten, V. Romero-Garcia, Multimodal reduction of acoustic radiation of thin plates by using a single piezoelectric patch with a negative capacitance shunt, Appl. Acoust. 145 (2019) 320–327..
[53] Y. Fan, M. Collet, M. Ichchou, L. Li, O. Bareille, Z. Dimitrijevic, A wave-based design of semi-active piezoelectric composites for broadband vibration control, Smart Mater. Struct. 25 (5) (2016) Article ID: 055032. doi:10.1088/0964-1726/25/5/055032..
[54] R. Darleux, B. Lossouarn, J.-F. Deú, Broadband vibration damping of non-periodic plates by piezoelectric coupling to their electrical analogues, Smart Mater. Struct. 29 (2020) Article ID: 054001..
[55] F. Xie, Y. Su, W. Zhou, W.-Z. Zhang, Design and evaluation of a shunted flexible piezoelectric damper for vibration control of cable structures, Smart Mater. Struct. 28 (8) (2019) Article ID. 085031. doi:10.1088/1361-665X/ab2c14..
[56] K. Billon, N. Montcoudiol, A. Aubry, R. Pascual, F. Mosca, F. Jean, C. Pezerat, C. Bricault, S. Chesné, Vibration isolation and damping using a piezoelectric flextensional suspension with a negative capacitance shunt, Mech. Syst. Signal Process. 140 (2020) Article ID: 106696. doi: 10.1016/j.ymssp.2020.106696..
[57] W. Tang, L.-B. Wang, Y.-M. Ren, B. Bao, J.-J. Cao, Design and experimental analysis of self-sensing ssdnc technique for semi-active vibration control, Smart Mater. Struct. 27 (8) (2018) Article ID: 085028. doi: 10.1088/1361-665X/aad0b9..
[58] H. Asanuma, T. Komatsuzaki, Nonlinear piezoelectricity and damping in partially-covered piezoelectric cantilever with self-sensing synchronized switch damping on inductor circuit, Mech. Syst. Signal Process. 144 (2020) Article ID: 106867. doi: 10.1016/j.ymssp.2020.106867..
[59] L. Yan, B. Bao, D. Guyomar, M. Lallart, Periodic structure with interconnected nonlinear electrical networks, J. Intell. Mater. Syst. Struct. 28 (2) (2017) 204–229, https://doi.org/10.1177/1045389X16649448.
[60] M. Berardengo, O. Thomas, C. Giraud-Audine, S. Manzoni, Improved resistive shunt by means of negative capacitance: new circuit, performances and multi mode control, Smart Mater. Struct. 25 (2016), Article ID: 075033.
[61] B. de Marneffe, A. Preumont, Vibration damping with negative capacitance shunts: theory and experiment, Smart Mater. Struct. 17 (3) (2008), Article ID 035015.
[62] J. Høgsberg, S. Krenk, Calibration of piezoelectric RL shunts with explicit residual mode correction, J. Sound Vib. 386 (2017) 65–81.
[63] M. Berardengo, S. Manzoni, A. Conti, Multi-mode passive piezoelectric shunt damping by means of matrix inequalities, J. Sound Vib. 405 (2017) 287–305.
[64] M. Berardengo, S. Manzoni, O. Thomas, M. Vanali, Piezoelectric resonant shunt enhancement by negative capacitances: optimisation, performance and resonance cancellation, J. Intell. Mater. Syst. Struct. 29 (12) (2018) 2581–2606.
[65] J. Toftekær, J. Høgsberg, Multi-mode piezoelectric shunt damping with residual mode correction by evaluation of modal charge and voltage, J. Intell. Mater. Syst. Struct. 31 (4) (2019) 570–586..
[66] O. Thomas, J.-F. Deü, J. Ducarne, Vibration of an elastic structure with shunted piezoelectric patches: efficient finite-element formulation and electromechanical coupling coefficients, Int. J. Numer. Methods Eng. 80 (2) (2009) 235–268.
[67] J. Høgsberg, Consistent frequency-matching calibration procedure for electromechanical shunt absorbers, J. Vib. Control 26 (13–14) (2020) 1133–1144.
[68] J.S. Hwang, H. Kim, J. Kim, Estimation of the modal mass of a structure with a tuned-mass damper using H-infinity optimal model reduction, Eng. Struct. 28 (1) (2006) 34–42.
[69] Evaluation of measurement data – guide to the expression of uncertainty in measurement, 2008, JCGM 100:2008..
[70] O. Thomas, C. Touzé, A. Chaigne, Asymmetric non-linear forced vibrations of free-edge circular plates. Part ii: experiments, J. Sound Vib. 265 (5) (2003) 1075–1101.
[71] L. von Wangeheim, Modification of the classical GIC structure and its application to RC-oscillators, Electron. Lett. 32 (1) (1996) 6–8.
[72] H. Van der Auweraer, P. Guillaume, P. Verboven, S. Vanlanduit, Application of a fast-stabilizing frequency domain parameter estimation method, J. Dyn. Syst. Measure. Control Trans. ASME 123 (4) (2001) 651–658, https://doi.org/10.1115/1.1410369.